Study of the microstructure of the grade 91 steel after more than 100.000h of creep exposure at 600°C

Clara Panait, Walter Bendick, A. Fuchsmann, Anne-Françoise Gourgues-Lorenzon, Jacques Besson

Study of the microstructure of the Grade 91 steel after more than 100,000h of creep exposure at 600°C*

C. Panait[1,2], W. Bendick[3], A. Fuchsmann[2], A.-F. Gourgues-Lorenzon[1], J. Besson[1]

[1]Centre des Matériaux, MINES ParisTech, UMR CNRS 7633, B.P. 87, 91003 Evry Cedex, France
[2] V&M France CEV, Route de Leval, B.P. 20149, 59620 Aulnoye-Aymeries, France
[3]Salzgitter Mannesmann Forschung GmbH, Ehinger Straβe 200, D-47259 Duisburg, Germany

Abstract:

This paper presents results on the evolution of microstructure (both matrix and precipitates) of an ASME Grade 91 steel that has been creep tested for 113,431h at 600°C under a load of 80MPa.

The microstructure was investigated using transmission electron microscopy (TEM) and revealed chromium rich $M_{23}C_6$ carbides, MX-type precipitates, Laves phases and modified Z-phases. Only a small amount of modified Z-phase was found. In order to quantify coarsening of precipitates and growth of new phases during creep, the size distributions of the identified precipitates were determined by analysis of TEM images. In addition to this, the size distribution of Laves phases was determined by image analysis of scanning electron micrographs.

Substructure modifications and creep damage were investigated on cross sections of the creep specimen using Electron Backscatter Diffraction and Scanning Electron Microscopy.

Keywords: P91 steel, creep, microstructure, Laves phases, modified Z-phase, SEM, TEM

1. Introduction

There are few published data available on the microstructure of 9-12% chromium heat resistant steels after nearly 100,000h of exposure to creep. Further development of new heat resistant steels such as ASME Grade 91 steel, presently successfully used for components in fossil power plants operating at temperatures around 550-600°C [1] rely on a better understanding of their long-term microstructural evolution. Previous works [2, 3, 4] presented data on the microstructure of the ASME P91 steel after long term creep exposure, but for exposure times lower than 100,000h.

It has been shown that extrapolation of short-term creep data (e.g. for lifetime lower than 10,000 hours) can lead to an overestimation of the creep strength after long term creep [5, 6, 7]. This overestimation is probably due to the metallurgical evolution of the steel during creep or damage development. This paper presents data on the microstructure of the Grade 91 after more than 100,000h of creep exposure, which will be useful for a better understanding of the loss of long-term creep strength.

2. Literature data on precipitate evolution in 9-12%Cr steels during creep

The microstructure of the as received ASME Grade 91 steel consists of a tempered martensite matrix with high dislocation density and precipitates. There are two kinds of precipitates: $M_{23}C_6$ (M=Cr, Fe, Mo) carbides located at prior austenite grain boundaries (PAGBs) and at other (packet, block, martensite lath) boundaries and finely dispersed MX-type (M=V, Nb and X= C, N) carbonitrides within laths. Carbides of type MC, M_2C [8] can be also identified in Grade 91 steels, but most of the precipitates present at boundaries (PAGBs, laths, blocks, packets) are $M_{23}C_6$ carbides.

There is a microstructural evolution of the ASME Grade 91 steel during creep exposure: precipitation of new phases (Laves phases, modified Z-phases), coarsening of precipitates (primarily $M_{23}C_6$ carbides) and recovery of tempered martensitic lath structure.

Intermetallic Laves phases precipitate during creep or aging. Their precipitation is observed after relatively short-term creep exposure at 600°C, for times shorter than 4,000h [9]. Laves phase

* Please cite this article in press as: Panait CG, et al., Study of the microstructure of the Grade 91 steel after more than 100,000 h of creep...,International Journal of Pressure Vessels and Piping (2010), doi:10.1016/j.ijpvp.2010.03.017

precipitation decreases the amount of Mo dissolved in the matrix, reducing solid solution strengthening. Quantitative studies on the evolution of the size of Laves phases during creep or aging have revealed a significant growth rate during the first 10,000h of exposure [10].

Modified Z-phase is a complex (Cr,Fe)(Nb,V)N nitride. Its composition for metal elements is 50 at.% (Cr + Fe) and 50 at.% (Nb+V) [11]. In the ASME Grade 91 steel, modified Z-phase formation is observed after very long term creep, for example after 34,141h, at 600°C, under a load of 100 MPa [12]. The precipitation of modified Z-phases is also reported in the heat-affected zone (HAZ) of welded joints [13, 14]. The modified Z-phase precipitation occurs at the expense of MX precipitates, possibly leading to partial or complete disappearance of those precipitates and suppression of MX-induced strengthening. For this reason, the modified Z-phase precipitation could be detrimental to service life of 9-12% Cr ferritic-martensitic steels. In fact, it was suggested to be the major cause of premature loss of creep strength of some 11-12% Cr heat resistant steels after relatively short term (<15,000h) creep [15]. It is more intense in the 11-12% Cr steels content than in 9% Cr steels [11]; for the ASME Grade 91 steel, the effect of precipitation of modified Z-phase on creep strength is not fully understood.

3. Experimental procedure

3.1. Materials

A broken P91 steel creep specimen with a rupture time of 113,431h at 600°C under a load of 80MPa and a sample from the same pipe in the as-received conditions (no thermal or creep ageing) were provided by Salzgitter Mannesmann Forschung GmbH, Germany. The pipe was 121 mm in outside diameter and 20 mm in wall thickness. Its chemical composition was (wt.%): 0.1C–0.36Si–0.41Mn–0.015P–0.003S–0.059N–0.022Al–8.43Cr–0.92Mo–0.04Cu–0.068Nb–0.11Ni–0.20V. The pipe had been given the following heat treatment: 1050°C for 60 min, air cooling followed by 730°C for 60 min and 750°C for 60 min, air cooling. The investigated creep specimen with a rupture time of 113,431 h at 600°C (80 MPa) exhibited an elongation of 7.3% and a reduction of area of 37 %. During creep the specimen showed a minimum creep rate of 1.8 10^{-7} (h^{-1}).

3.2. *Transmission electron microscopy (TEM) investigations*

TEM investigations were performed with a Tecnai F20 transmission electron microscope. TEM investigations were carried out on single carbon extractive replicas and thin foils. The carbon replicas of precipitates were prepared as follows. First, the creep sample was polished and Villela etched. Then, a carbon coating was evaporated onto the polished and etched surface; after that the sample was immersed in a 1% HCl solution in methanol to detach the carbon layer from the specimen. The carbon replicas were recovered on round copper grids. Thin foils from the gauge part of the creep specimen were prepared combining electropolishing and ion beam milling. An acid solution (45% acetic acid, 10% perchloric acid, 45% Butoxyethanol) cooled down to -1°C was used for electropolishing. The electropolished foils were further thinned by ion beam milling for a few minutes at low angle using a Gatan Precision Ion Polishing System (PIPS).

The chemical composition of each precipitate was determined by Energy dispersive X-Ray spectrometry (EDX) in conjunction with TEM. The identification was done using the following criteria: $M_{23}C_6$ carbides are enriched in Cr, Laves phases are enriched in Mo, modified Z-phase are made out of ~50 at.% (Cr + Fe) and ~50 at.% (V+Nb) and MX are enriched in V and Nb. More than 600 precipitates were investigated on several extractive replicas.

It is not sure that all precipitates are extracted on the carbon replica. As a consequence, special attention was paid to select an investigation area that was representative of the microstructure of the steel after etching.

Literature reports an average diameter of MX precipitates of 20 to 40 nm [16]. MX-type precipitates were identified on investigated extractive replicas; nevertheless, attention was focused to identify only larger precipitates after long-term creep, which could have a significant influence on the loss of creep strength. Thus, EDS analyses were mainly conducted on precipitates with an average diameter higher than 90 nm. MX–type precipitates were observed on thin foils.

3.3. *Scanning electron microscopy (SEM) investigations*

Creep damage was investigated using a Scanning Electron Microscope (SEM) (Leo 1450 VP, with a tungsten filament) on longitudinal cross sections. One broken half of the creep specimen was cut into two halves (i.e. quarters of "complete" specimens) by spark erosion. The half containing the specimen axis was used for metallographic examinations. A final mechanical-chemical polishing with colloidal silica was then carried out to reveal cavities without opening them, as chemical etching could have done. The creep damage was quantified as a fraction of porosity determined by image analysis of SEM images with a magnification of ×400.

3.4. Electron Backscatter Diffraction (EBSD) investigations

Electron backscatter diffraction (EBSD) maps were acquired from the same cross-section with a Zeiss DSM 982 Gemini field emission gun (FEG) SEM equipped with a Shottky filament, a Hjelen-type camera and TSL OIM facilities. The specimen for EBSD maps was also polished with colloidal silica. All EBSD measurements were conducted with a step size of 0.15 µm at 20kV, working distance 19 mm, aperture 120 µm, probe current between 0.1 and 1nA.

The EBSD maps were acquired together with a backscattered electron (BSE) image (taken at 0° specimen tilt), where the contrast is highly sensitive to the crystallographic orientation of the sample normal (i.e., of the primary electron beam). Laves phases, enriched in Mo, are also clearly visible thanks to their high average atomic number.

The first map built after EBSD data processing is the "image quality" map, which reports, for each analysed point, the ability of the software to detect the diffraction bands. The brighter the grey level, the better the diffraction conditions. Image quality is sensitive to the crystal orientation, as well as to the "channelling effect" that yields the BSE image contrast. In addition, image quality is very sensitive to crystal defects such as dislocations. As soon as dislocations are clustered somewhere, the EBSD pattern quality decreases. Thus, the image quality map is very sensitive to the presence of boundaries, *even for very low angle boundaries.*

Inverse pole figure (IPF) maps were colour-coded according to the orientation of a given direction of the sample in the crystal frame. The colour key is recalled next to each IPF map.

In addition to IPF mapping, one may calculate the misorientation between neighbouring pixels and assign a colour code to any pair of pixels whose misorientation meets a given criterion. This helps investigations whether a "boundary" imaged in the image quality maps corresponds to a high or to a low misorientation angle, or even to negligible misorientation between neighbouring crystals. This is particularly useful to investigate subgrain boundaries. In all maps, the colour code for boundaries is recalled according to the misorientation angles.

4. Creep damage

A high number density of cavities was observed throughout the specimen section even far from the fracture surface, using either backscatter electron (BSE) or secondary electron (SE) imaging (Figure 1). Many cavities can even be observed using a light microscope.

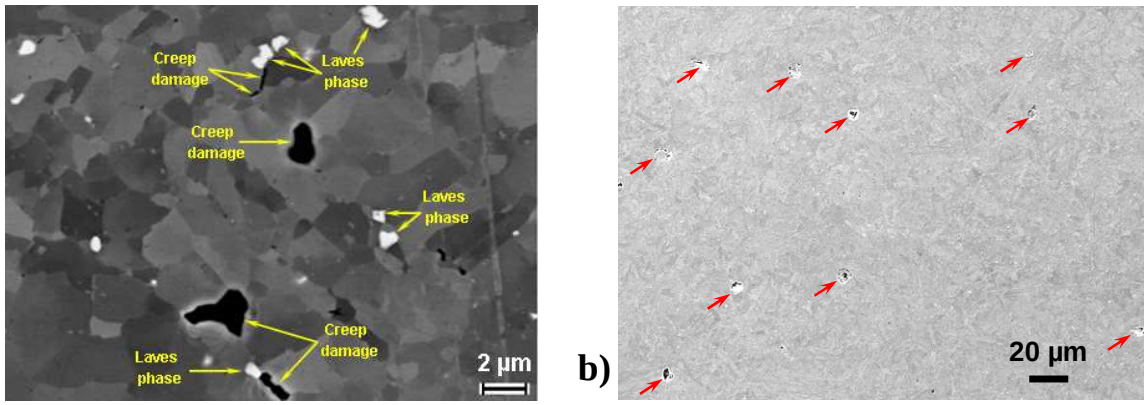

Figure 1 *Creep damage in the P91 steel after creep at 600°C for 113,431h 7mm from fracture surface, SEM images, BSE-mode (a) and SE-mode (b)*

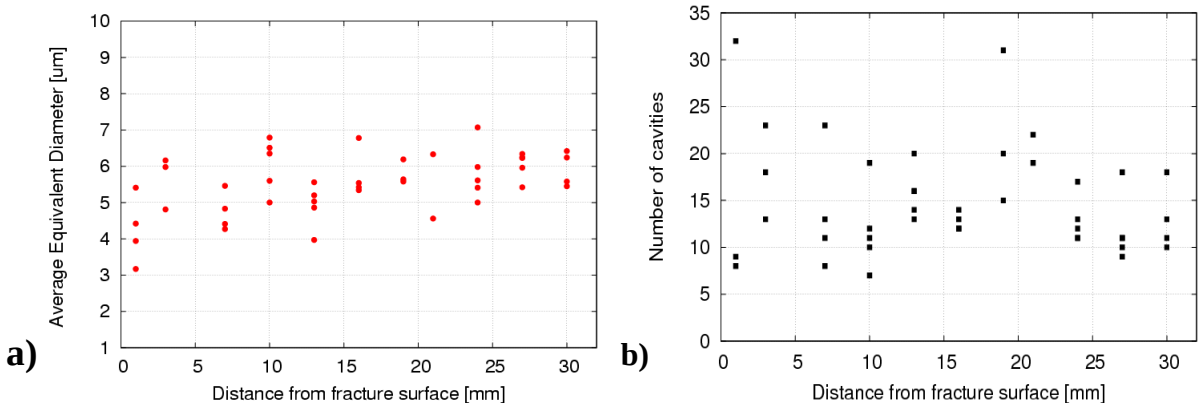

Figure 2 *Average equivalent diameter (a) and number of cavities (b) calculated on areas of 342µmx214µm along the creep specimen axis*

Figure 2 reports data on the average equivalent diameter of cavities and number of cavities observed at a magnification of ×400. At this magnification cavities with a minimum equivalent diameter of 0.7 µm can be revealed. Creep damage was quantified on areas of 342µm×214µm. In figure 1b is represented a typical SEM image used for creep damage quantification, arrows show creep cavities. Cavities seem to nucleate at boundaries next to large particles such as Laves phases (Figure 1a). At a distance lower than about 0.5mm from the fracture surface, coalescence of cavities was observed.

5. Hardness

The gauge portion of the investigated creep specimen exhibits hardness with about fifty units lower than in the as-received P91 steel. This decrease in hardness can be due to both the presence of cavities and microstructural evolution of the steel during creep. Close to the fracture surface, one observes a slight decrease in hardness compared to that of the rest of the gauge portion of the specimen. This can be related to creep damage development. The head of the creep specimen shows a lower decrease in hardness, about twenty units lower than the as received P91 steel. This small decrease is probably due to microstructural evolution.

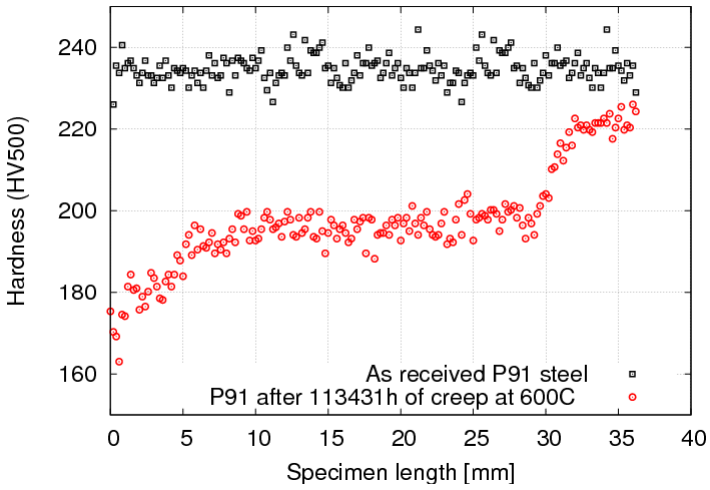

Figure 3 *Evolution of hardness along the tensile direction of investigated creep specimen (circles) compared to that of a similar piece of as-received steel from the same pipe (squares)*

The difference in hardness between gauge and specimen head could be due to either the effect of stress on microstructural evolution or damage development, or both. Thus, three states of the microstructure of the P91 steel were investigated:

- the as received state,
- the head of the creep specimen (stress-free thermal ageing),
- the gauge portion far from fracture surface (microstructural evolution under stress/strain).

6. Microstructural evolution during creep

6.1 Scanning Electron Microscopy results (Laves phases)

In the as-received state, precipitates are too small to be analysed using SEM. The precipitates that can be seen in Figure 4a are $M_{23}C_6$ carbides mainly located at boundaries. There are also small MX-type precipitates finely distributed within the martensite laths and Mo atoms in solid solution in the matrix.

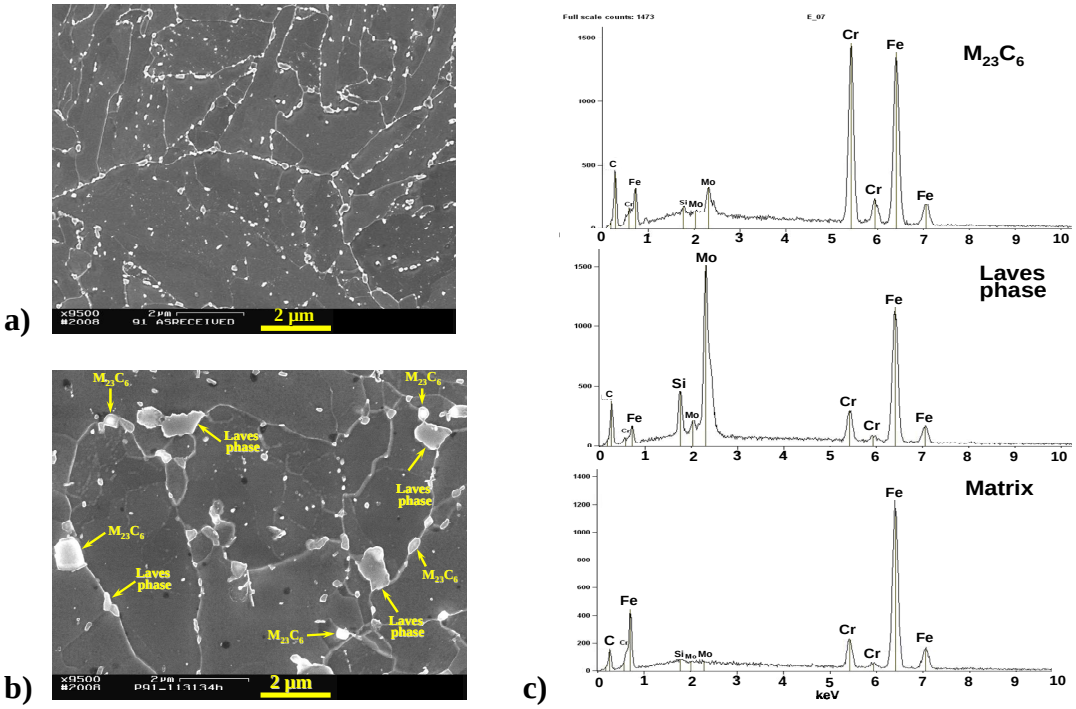

Figure 4 *Microstructure of the a) as received P91, b) after creep at 600°C for 113,431h (gauge); c) typical EDS (FEG-SEM) spectra for $M_{23}C_6$ carbides, Laves phases and matrix, respectively*

After long-term creep, $M_{23}C_6$ carbides have obviously grown (Figure 4). FEG-SEM investigations revealed precipitation of Laves phases. Small-size precipitates (~40nm) finely distributed was also observed by FEG-SEM in the crept specimen. They were too small to be identified by FEG-SEM; they could be MX-type precipitates. To study this kind of precipitates, TEM investigations are needed.

The precipitates indicated in Figure 4b were identified by EDS analysis coupled with FEG-SEM. The large size of some precipitates after long-term creep allowed their chemical identification by EDS analysis (Figure 4c).

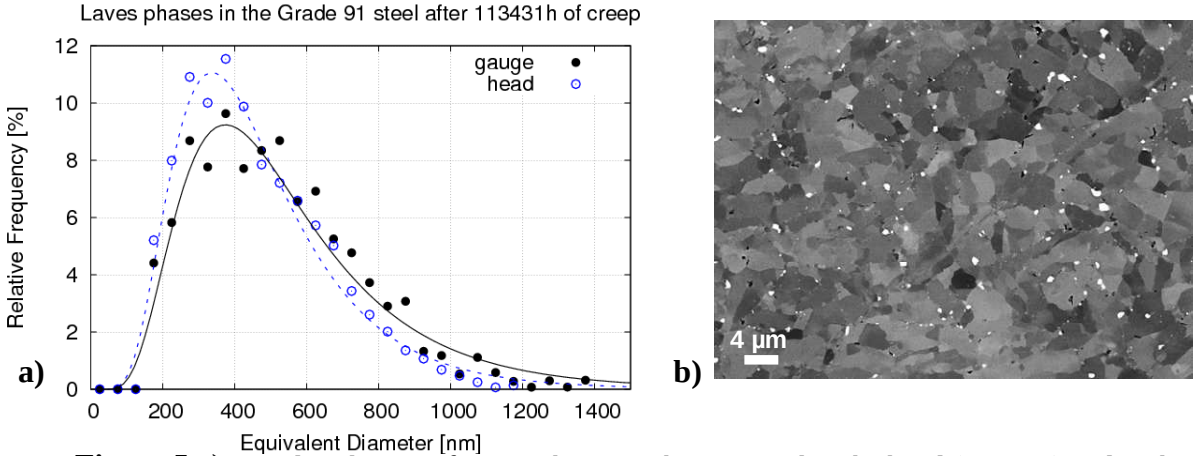

Figure 5 a) *Size distribution of Laves phases in the P91 steel in the head (squares) and in the gauge portion (circles) of the creep specimen; b) Microstructure of the P91 steel after creep, showing Laves phases (white)*

Figure 5a shows the size distribution of Laves phases after creep. Because Laves phases are enriched in Mo, they can be easily evidenced using BSE images, which are sensitive to the mean atomic number of the probe area. Figure 5b shows a typical BSE image used for quantification of Laves phases, white spots being Laves phase particles. The precipitation of Laves phases occurs during high-temperature exposure; in the as-received state there are no Laves phases, as can be seen in the micrograph of Figure 6a.

There is no significant difference between the size of Laves phases in the gauge portion compared to the head portion. The slight difference between curves of Figure 5a could be due to the scatter of measurements.

6.2 Electron Backscatter Diffraction results (Grain/subgrain structure)

SEM-BSE investigations revealed a significant change in the substructure of the steel after long-term creep, as can be seen from Figure 6 compared to Figures 8, 10 and 12.

EBSD maps of the steel in as-received state revealed a typical martensitic matrix with blocks and packets. After creep, EBSD measurements revealed a matrix with more or less equiaxed subgrains (Figures 8b, 10b, 12b). These subgrains are revealed by both BSE imaging and EBSD mapping. The shape of these subgrains is very elongated in the as received state (Figure 7a) and less elongated in the specimen head (Figure 13a). In the specimen gauge, at 25 mm from the fracture surface, equiaxed subgrains are readily found (arrows in Figure 11a). Next to the fracture surface, most subgrains are round-shaped (Figure 9a).

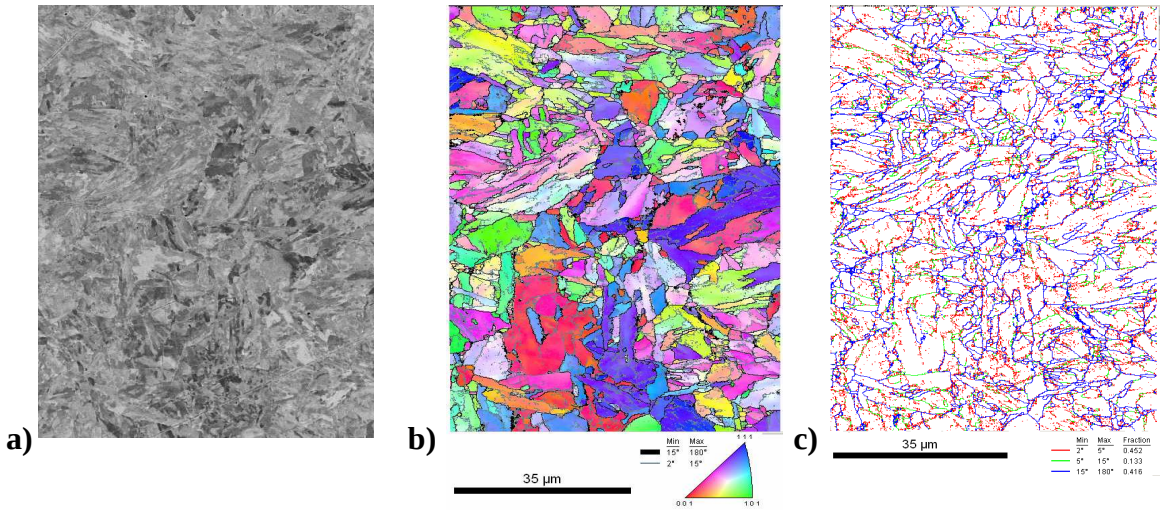

Figure 6 *Microstructure of the as-received P91 steel.*
a) SEM-BSE micrograph; b) Inverse Pole Figure (IPF) with orientation of sample normal in the crystal frame as key colour; c) EBSD Boundary map;

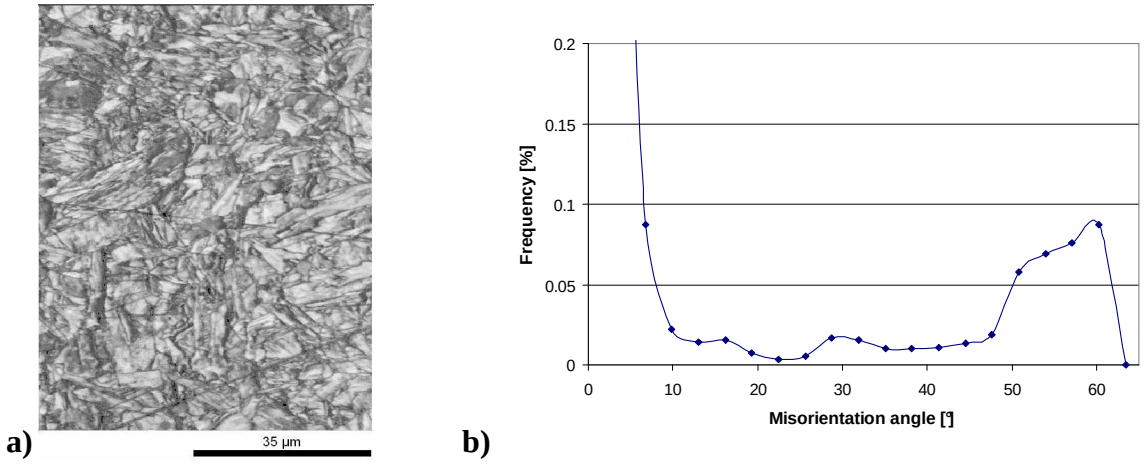

Figure 7 *EBSD Image Quality map (a) and misorientation angles for EBSD maps in figure 6*

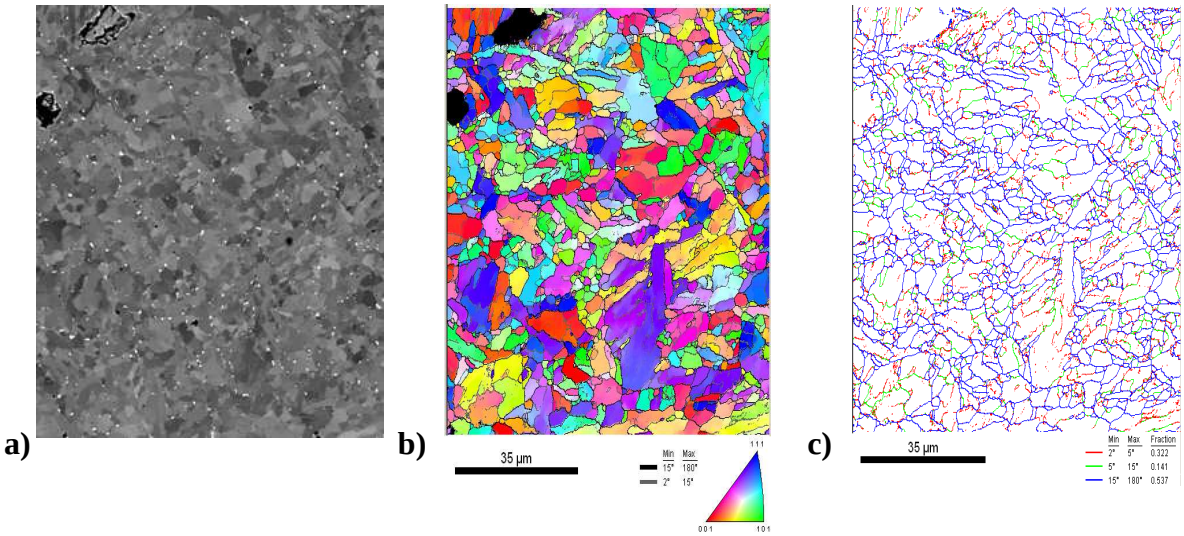

Figure 8 *Microstructure of P91 steel after 113431h of creep at 600°C (2mm from fracture surface) a) SEM-BSE micrograph; b) Inverse Pole Figure (IPF) with orientation of sample normal in the crystal frame as key colour; c) EBSD Boundary map.*

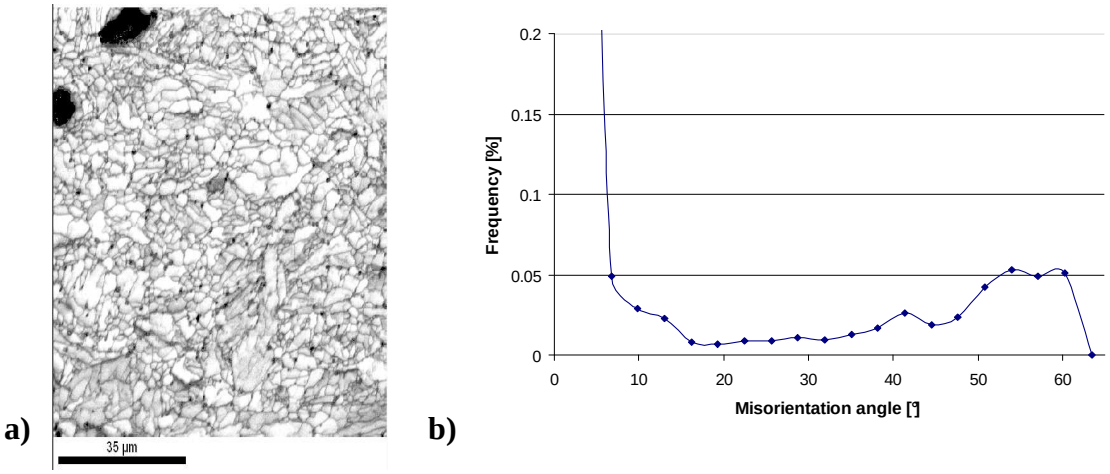

Figure 9 *EBSD Image Quality map (a) and misorientation angles (b) for EBSD maps in figure 8*

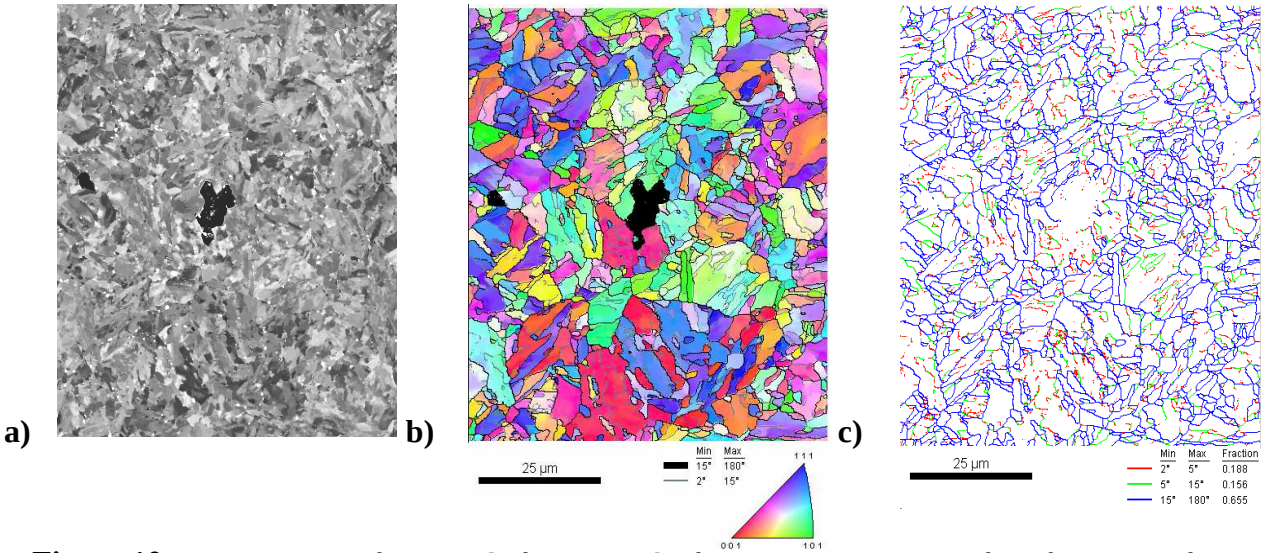

Figure 10 *Microstructure of P91 steel after 113431h of creep at 600°C (25mm from fracture surface) a) SEM-BSE micrograph; b) Inverse Pole Figure (IPF) with orientation of sample normal in the crystal frame as key colour; c) EBSD Boundary map.*

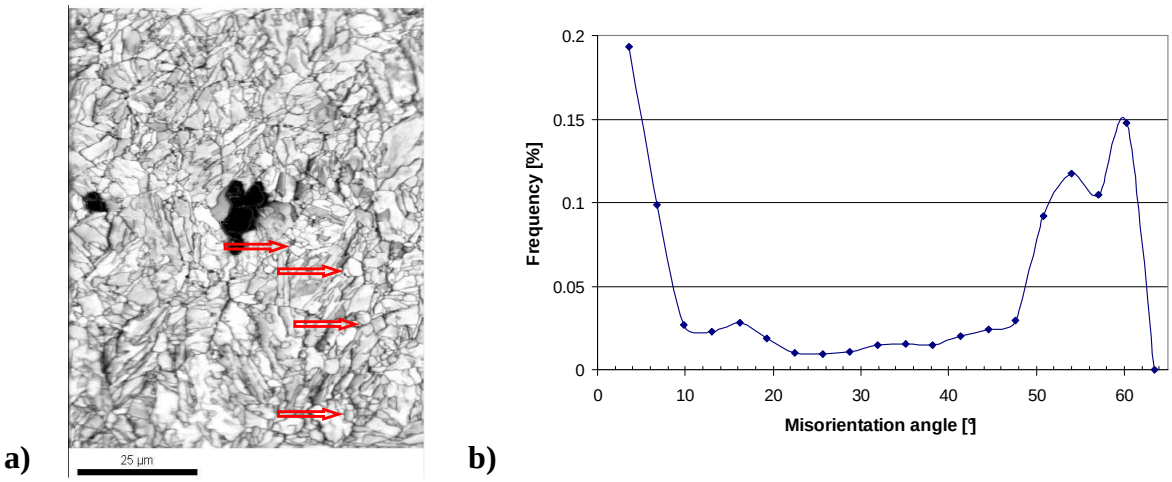

Figure 11 *a) EBSD Image Quality map some equiaxed subgrains are arrowed; b) misorientation angles (b) for EBSD maps in figure 10*

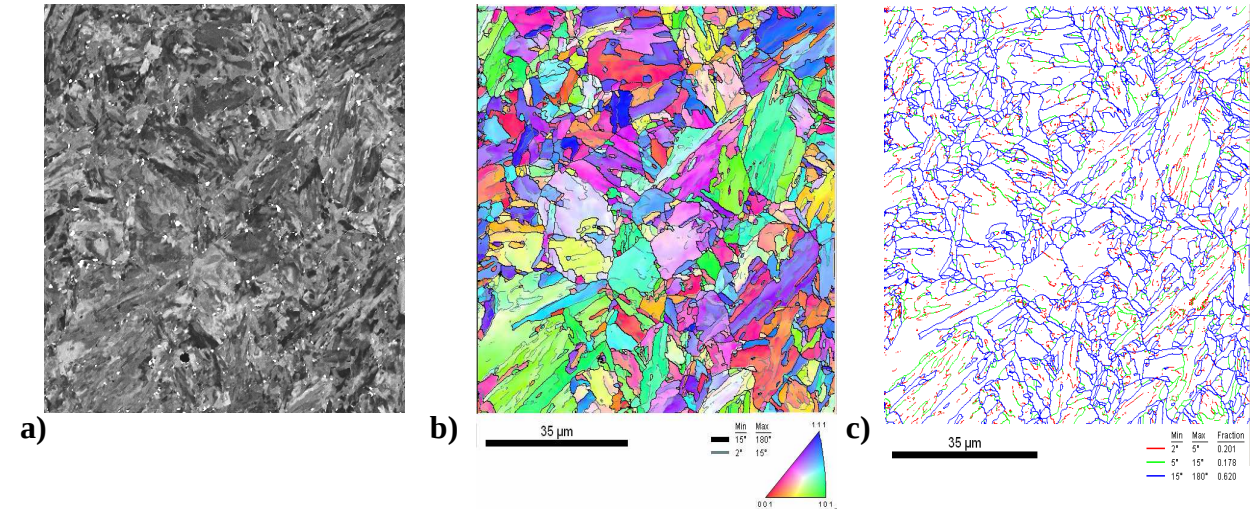

Figure 12 *Microstructure of the P91 steel after 113431h of creep at 600°C (head of the specimen) a) EBSD IPF (same colour key as in Figure 6a); b) BSE image; c) EBSD Image Quality map*

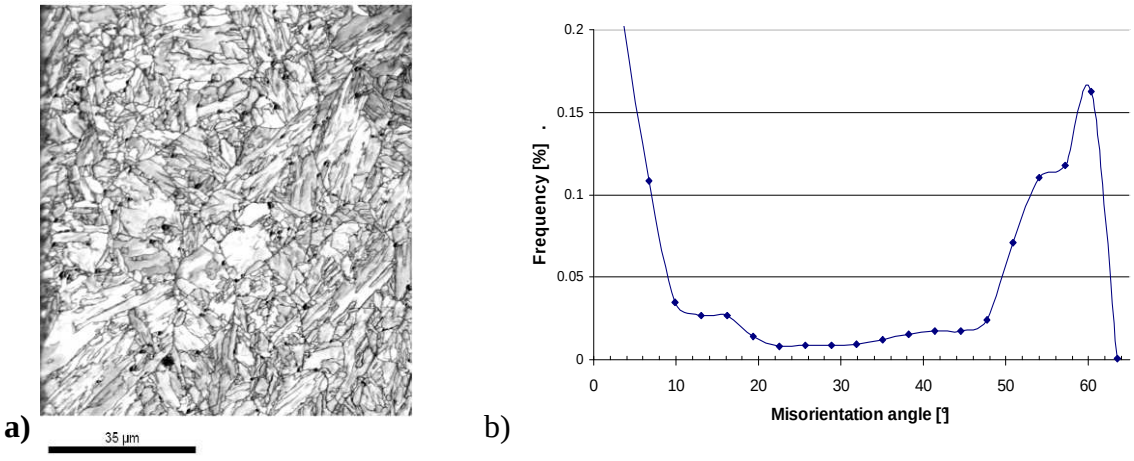

Figure 13 *EBSD Image Quality map (a) and misorientation angles (b) for EBSD maps in figure 12*

Subgrain evolution occurred both upon thermal aging (head) and creep deformation (gauge) but probably mostly during fast deformation immediately proceeding fracture. To assess the metallurgical evolution of the creep specimen it is necessary to separately study what occurred during creep deformation (homogeneously deformed area, Figure 10) and what is due to fast "quasiplastic" deformation at the end of lifetime (next to fracture area, Figure 8). First of all, as creep cavities are

uniformly distributed along the gauge length (see figure 2), it can be concluded that extensive recovery leading to round-shaped subgrains is not necessary to induce premature creep failure.

In addition, small equiaxed grains (a few microns in size) delimited by high-angle boundaries (>15°) were revealed in the EBSD maps (Figures 8b, 10b, 12b) although they could not be clearly identified by BSE imaging. Such grains were not so obviously detected in the as received state (Figure 6) and must have appeared during creep.

Misorientation angle histograms of figures 7b, 9b, 11b, 13b showed that while in figures 7b, 11b and 13b boundaries between small grains have misorientation angles typical of those between martensite variants from the same parent austenite grain [17, 18], this might be not so clearly the case 2 mm from the fracture surface (figure 9b). This suggests that some continuous recrystallisation might have occurred close to the fracture surface. This is consistent with dynamic recrystallisation occurring in another P91 steel fractured in tension ($10^{-3}s^{-1}$) at 625°C [19]. Getting more information about this phenomenon requires more detailed EBSD data processing that is beyond the scope of this paper.
Note that this phenomenon occurs just before failure and does not influence lifetime.

6.3 Transmission Electron Microscopy results (Modified Z-phase and $M_{23}C_6$ carbides)

The main purpose of TEM investigations was to determine the size and number density of modified Z-phase particles in order to decide how to take into account the influence of this phase on the creep strength of the ASME Grade 91 steel.

As Laves phases are large and relatively scarcely distributed, more representative data on the size of Laves phases can be obtained using SEM (see Figure 5a). Thus, to determinate the sizes of relative large precipitates such as Laves phases, SEM is better suited [22] because of the possibility of a higher number of precipitates per image, which allows better statistics compared to TEM images. However, TEM is better suited to investigation of modified Z-phases, which are frequently located very close to other particles, so that good spatial resolution is needed to analyse them.

TEM is also better suited for the characterization of $M_{23}C_6$ carbides, due to their small size (an average equivalent diameter of 90-100nm in as received Grade 91 steel).

6.3.1 Modified Z-phase

Figure 14a shows typical precipitates in the P91 steel after long term creep exposure. TEM investigations revealed a low number of modified Z-phase particles compared to the size of the investigated area or the number of investigated precipitates. Only 41 precipitates out of 640 identified precipitates were found to be modified Z-phases. The observed modified Z-phases are large and widely spaced particles with a mean diameter going from 250nm to 750nm.

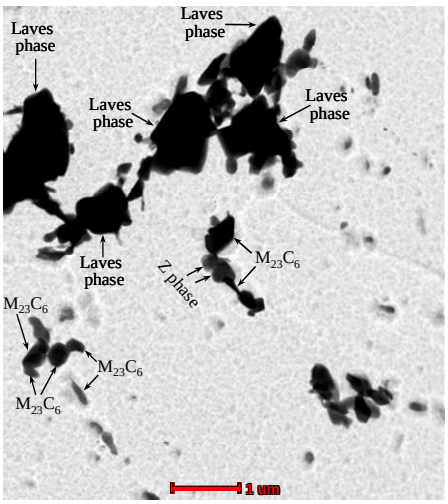

a)

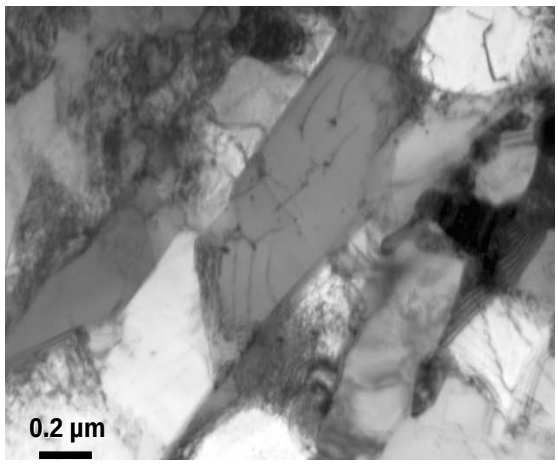

b)

Figure 14 *Microstructure of the steel after creep; a) extractive replica; b) thin foil*

Precipitation of modified Z-phase can put the MX-type precipitates into solid solution. However, TEM investigations on thin foils of the crept portion revealed dislocations still pinned by MX-type precipitates as shown in Figure 14b. This suggests that precipitation of modified Z-phase did not have a significant influence on the number density of MX-type precipitates; nevertheless, no quantification of MX-type precipitates was done in this study.

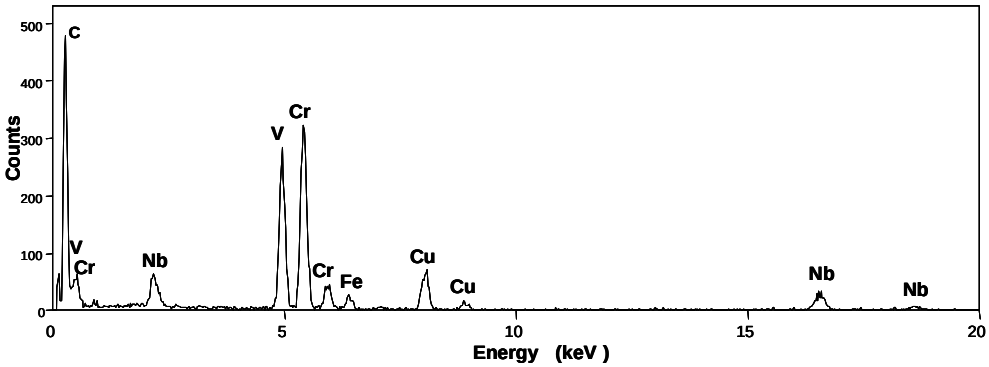

Figure 15 *Typical EDX-TEM spectra for modified Z phase*

As mentioned above, the identification of modified Z phase was based mainly on its chemical composition of about ~50 at.% (Cr + Fe) and ~50 at.% (V+Nb) (metal elements only). Figure 15 shows a typical EDX-TEM spectrum for modified Z-phases. Table 1 summarizes EDX results on modified Z-phases identified on extractive replicas of the creep specimen (gauge portion). The Cr/Fe ratio was uniform with around 46 at.% Cr and 4 at.%. Fe. The V and Nb contents showed large scatter. Danielsen and Hald [20] found similar variations of Cr/Fe ratio and Nb/V ratio in chemical composition of modified Z-phases of various 9-12%Cr martensitic steels.

Table 1 Average chemical composition of modified Z-phase found in the P91 steel after 113431h of creep at 600°C

	Cr		**Fe**		**V**		**Nb**	
	%at.	%wt.	%at.	%wt.	%at.	%wt.	%at.	%wt.
Min	41.1	34.9	2.1	2.1	30.9	26.4	4.2	7.3
Max	50	47.6	7.7	8.0	45.2	42.5	23.3	35.3
Average	**46.5**	42.9	**3.8**	3.8	**38.2**	34.7	**11.3**	18.4
Standard deviation	2.2	2.9	1.1	1.1	4.1	4.6	4.6	6.9
Danielsen and Hald [19]	45		5		40		10	

Number of EDX analysis (modified Z-phase particles): 33

6.3.2 $M_{23}C_6$ carbides

Table 2 summarizes EDX results on $M_{23}C_6$ carbides in the as-received state and after long-term creep. A change in average chemical composition of the $M_{23}C_6$ particles after creep can be observed. For metal elements, an increase in Cr content from about 60 at.% to 70 at.% and a decrease in Fe content from about 30 at.% to 20 at.% are observed in the crept specimen.

Table 2: Synthesis of EDX analysis of $M_{23}C_6$ carbides on single extractive replicas (%at.)

	As received						After 113431h of creep at 600°C				
	Cr	**Mo**	**Fe**	**Mn**	**V**		**Cr**	**Mo**	**Fe**	**Mn**	**V**
Minimum	55.2	0	21.4	0	0		61.4	4.0	11.6	1.0	0
Maximum	67.9	10.7	39.7	7.8	5.6		77.6	11.9	21.4	10.9	1.3
Average	**61.2**	**5.7**	**27.7**	**4.8**	**0.1**		**70.5**	**6.8**	**17.0**	**5.3**	**0.1**
Standard deviation	2.8	1.6	2.1	2.0	0.6		3.6	1.5	2.0	2.3	0.2
	Number of investigated carbides: 128						Number of investigated carbides:120				

K. Kimura et al. [21] found the same change in chemical composition of the $M_{23}C_6$ in a Grade 91 steel with an exposure time to creep of 34,000h at 600°C. In the as-received state, the chemical composition of the $M_{23}C_6$ determined in this study is similar to those determined in a similar steel [21].

Figure 16 shows the size distribution of $M_{23}C_6$ carbides identified on extractive replicas by EDX-TEM in the as-received P91 steel end after creep at 600°C. A growth in size of $M_{23}C_6$ carbides is observed after creep. The average equivalent diameter of $M_{23}C_6$ carbides increases from about 150-180nm to about 300nm.

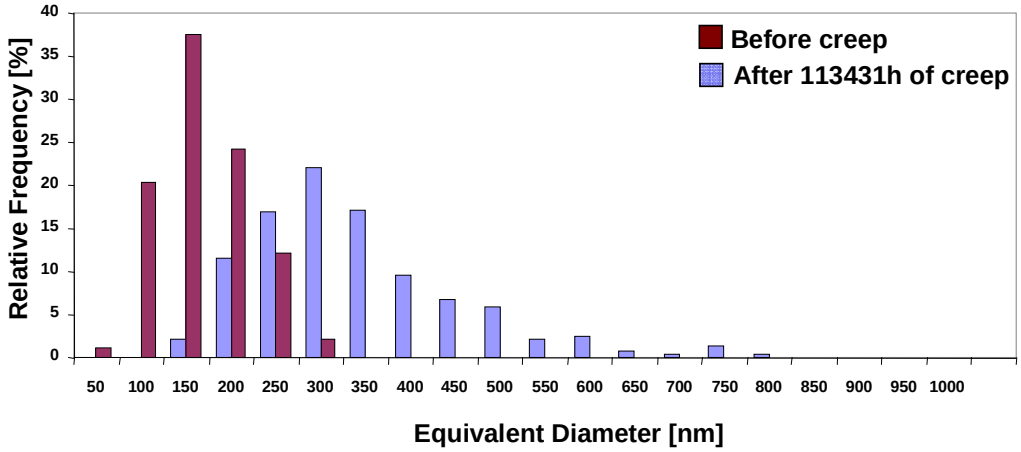

Figure 16 *Size distribution of $M_{23}C_6$ carbides in the as received P91 steel and after113431h of creep at 600°C (carbides identified on extractive replicas of precipitates)*

7. Conclusions

Quantitative data on the microstructure (both matrix and precipitate) of P91 steel after long-term creep were obtained in this study. After creep for 113,431h at 600°C, significant coarsening of existing $M_{23}C_6$ carbides, as well as intensive precipitation of coarse Laves phases and a low amount of modified Z-phases were observed.

The investigated creep specimens showed a significant decrease in hardness on the gauge area and a reduced decrease in the head. Creep damage was observed throughout the gauge area, next to coarse Laves phases.

A significant change in the substructure of the matrix was revealed by EBSD measurements. It was accelerated by creep compared to thermal ageing, but no extensive recrystallisation occurred prior to necking. Dislocation pinning by MX precipitates was still observed in the crept area.

This paper suggests that loss of creep strength is probably mainly due to coarsening of $M_{23}C_6$ carbides, significant precipitation and coarsening of Laves phases, and significant recovery of the matrix, rather than to extensive precipitation of modified Z-phase and significant MX dissolution.

Acknowledgments

Authors would like to thank Dr. Ing. Frédéric Delabrouille, from EDF, Renardières for TEM observations on thin foils. Authors will also like to thank Dr. Ing. Mohamed Sennour from Centre des Matériaux for his precious advises with carrying on TEM investigations. Dr. Ing. Francois Grillon from Centre des Matériaux is also acknowledged for kind technical support with conducting EBSD investigations.

References

1. Rukes B., Taud R., Status and perspectives of fossil power generation, Energy 29 (2004) 1853-1874
2. Hald J., Korcakova L., Precipitate stability in creep resistant ferritic steels–experimental investigations and modelling, ISIJ International 43 (2003) 420-427
3. Sawada K.et al., Contribution of microstructural factors to hardness change during creep exposure in mod.9Cr-1Mo steel, ISIJ International 45 (2005) 1934-1939
4. Cipolla L., et al., Long term creep behaviour and microstructural evolution of E911 steel, Proceedings of ECCC Creep Conference, 12-14 sept. 2005, London, Edited by I.A. Shibli, S.R. Holdsworth, G. Merckling, pp. 288-299 ISBN 1-932078-49-5
5. Abe F., Bainitic and martensitic creep-resistant steels, Current Opinion in solid State & Materials Science 8 (2004) 305-311
6. Bendick W. and Gabrel J., Assessment of creep rupture strength for the new martensitic 9%Cr steels E911 and T/P92, Proceedings of ECCC Creep Conference, 12-14 sept. 2005, London, Edited by I.A. Shibli, S.R. Holdsworth, G. Merckling, pp.406-427, ISBN 1-932078-49-5
7. Gaffard V., Gourgues-Lorenzon A.-F., Besson J., High temperature creep flow and damage properties of 9Cr1MoNbV steels: Base metal and weldment, Nuclear Engineering and Design, 235 (2005), 2547-2562
8. Kaneko K., Matsumura S., Sadakata A., Fujita K., Moon W. –J., Ozaki S., Nishimura N., Tomokyio Y., Characterization of carbides at different boundaries of 9Cr-steel, Materials Science and Engineering A374 (2004) 82-89
9. Hald J., Creep strength and ductility of 9 to 12% chromium steels, Materials at high temperature 21 (1) 41-46, 2004
10. Dimmler G., et al., Quantification of Laves phase in advanced 9-12%Cr steels using a standard SEM, Materials Characterization 51 (2003) 341-352
11. Danielsen H., Hald J., A thermodynamic model of the Z-phase Cr(V,Nb)N, Computer coupling of phase diagrams and thermochemistry 31 (2007) 505-514
12. Kimura K., Kushima H., Abe F., Suzuki K., Kumai S., Satoh A., Microstructural change and degradation behaviour of 9Cr-1Mo-V-Nbsteel in the long term, Proceedings of the 5th International Charles Parson Conference, 3-7 July 2000, Cambridge, UK, pp. 590-602, Edited by: A. Strang et al., ISBN 1-86125-113-0
13. Abd El-Azim M.E., Nasreldin A. M., Zies G., Klenk A., Microstructural instability of a welded joint in P91 steel during creep at 600°C, Materials Science and Technology 21 (2005) 779-790
14. Letofsky E., Cerjak H., Papst I., Warbichler P., The use of ligth and electron-microscopic investigations to characterise the creep bhaviour of welded joints in modern power station materials, Proceedings of the 3rd Conference on Advances in Material technology for fossil power plants, Swansea, 2001, pp. 133-142, Edited by: R. Viswanathan, W.T. Bakker, J.D. Parker, ISBN 1-86125-145-9
15. Uehara T., et al., Improvement of creep rupture strength of high strength 12Cr ferritic heat-resistant steel, Proceedings of the Conference on the “Materials for Advanced Power Engineering” (2002), pp. 1311-1320, Eds. J. Lecomte-Beckers et al., Forschungszentrum Jülich, Liège, ISBN 3-89336-312-2
16. Gustafson A., Hättestrand M., Coarsening of precipitates in an advanced creep resisitant 9% chromium steel – quantitative microscopy and simulations, Materials Science and Engineering A333 (2002) 279-286
17. S. Morito et al., The morphology and crystallography of lath martensite in alloy steels, Acta Materialia 54 (2006) 5323-5331
18. Gourgues, A.-F., Flower H. M. and Lindley T.C., Electron backscattering diffraction study of acicular ferrite, bainite and martensite microstructure, Materials Science and Technology 16 (2000) 26-40
19. Gaffard, V., Experimental study and modelling of high temperature creep flow and damage behaviour of 9Cr1Mo-NbV steel weldments, p. 34, Ph.D thesis, 2004, Ecole des Mines de Paris, France (in English)
20. Danielsen H., Hald J., Behaviour of Z phase in 9-12%Cr steels, Energy Materials 1 (2006), 49-57

21. Kimura K.et al., Precipitation of Z-phase and degradation behaviour of mod. 9Cr-1Mo steel, Proceedings of the Conference Materials for Advanced Power Engineering (2002), pp. 1171-1180, eds. J. Lecomte-Beckers et al., Julich Forschungszentrum, Liège ISBN 3-89336-312-2
22. Andren H.-O., Combining TEM and APFIM techniques to study the microstructure of steels and hardmetals, Micron 32 (2001) 713-719